PHYSICAL REVIEW A VOLUME 10, NUMBER 5 NOVEMBER 1974

# Alkali-metal negative ions. I. Photodetachment of $Li^-$, $Na^-$, and $K^-$[†]

D. L. Moores* and D. W. Norcross
*Joint Institute for Laboratory Astrophysics, University of Colorado and National Bureau of Standards, Boulder, Colorado 80302*
(Received 6 June 1974)

Photodetachment cross sections of the negative ions of the three lightest alkali-metal atoms have been calculated using configuration-interaction wave functions for the initial state and close-coupling scattering wave functions for the final state. Pronounced structure obtained at the threshold for leaving the neutral atom in the first excited state is due to a combination of real resonance behavior and the threshold law for collisional excitation. The range of validity of this law is, however, found to be very narrow. The shape of the cross sections in this region is in excellent agreement with experimental measurements. Results are also presented for the angular distribution of the photoelectrons following photodetachment with simultaneous neutral excitation, for the dipole polarizabilities of the negative ions, and simple analytic formulas for the radiative attachment coefficients.

## I. INTRODUCTION

Reliable estimates of the electron affinities and photodetachment cross sections of the alkali-metal negative ions are required for interpretation of the properties of low-temperature plasmas, and in the fields of upper-atmosphere physics and astrophysics. In addition, accurate electron affinities would provide extremely useful benchmarks for obtaining affinities of other elements in the Periodic Table by interpolation or extrapolation techniques.

Until very recently, experimental data on the electron affinities of the alkali metals has been very limited both in quantity and quality. Theoretical results are more plentiful, and have a greater degree of mutual consistency than the experimental data. Citations of almost all values obtained to date can be found in Refs. 1–4.

Theoretical values for the electron affinities have been obtained both from semiempirical extrapolations of known spectral data, and from atomic-structure calculations of varying degrees of complexity. The essential feature in these latter calculations seems to be the inclusion of configuration interaction, the work of Weiss[5] being the most sophisticated (*ab initio*, variational Hartree-Fock) calculation of this type. Most calculations neglect, however, the effect of core polarization, which has been shown to be large for the heavy alkali metals.[6] In this calculation, the electron affinities of all of the alkali-metal atoms were obtained in a novel application of the coupled equations of scattering theory, using semiempirical effective potentials for the neutral alkali-metal atoms.

The measurements have employed a number of methods, e.g., exploding wires, surface ionization, and resonant charge exchange, all of which are subject to large uncertainties. Practical problems such as the wavelength region of the expected onset of photodetachment [$(2-3)\times 10^4$ Å] and the difficulty of getting a sufficiently high density of negative ions have hindered application of standard photoabsorption techniques. The development in recent years of photodetachment techniques which include the counting of reaction particles provides the opportunity for much more direct and accurate measurements. The accuracy of results obtained using a conventional arc light source[7] is limited primarily by energy resolution, which would be particularly troublesome in the case of the alkali-metal negative ions since the derivative of the cross section at threshold with respect to photoelectron energy is zero. The development of tunable dye lasers led to a technique[8] capable of yielding much greater precision in measured electron affinities, limited primarily by counting statistics, provided that threshold is accessible or that a sharp feature in the cross section can be unambiguously identified as a known spectroscopic state.

The results of several calculations[9–11] for scattering of electrons by neutral alkali metals suggest that the electron affinities of the alkali-metal negative ions might be accurately measured using the dye-laser photodetachment method. The significant feature of these results is very pronounced structure in the $^1P^0$ partial-wave cross section for elastic scattering near the first excitation threshold. This structure is partly due to the opening of a new channel with electron angular momentum $l=0$, the so-called "Wigner cusp" (which occurs for both the $^1P^0$ and $^3P^0$ partial waves), combined with what appears to be real resonant behavior. This threshold behavior will be studied in some detail in Sec. II C, the essential result being that the derivative with respect to electron energy of the $^1P^0$ partial cross section for elastic scattering from the ground state

is infinite at the first excitation threshold, leading to a cusp or a step in this cross section at threshold, which is greatly enhanced by a resonance.

Now considering the photodetachment process, since the ground state of the alkali-metal negative ions is assumed to be a $^1S$ state, the final continuum state must be a $^1P^0$ state according to the dipole selection rule. The final state may also be regarded as the electron-neutral scattering system in the $^1P^0$ partial wave. Any structure in the partial scattering cross section should therefore be reflected in the photodetachment cross section at photon energies corresponding to ejection of an electron with energy equal to the first excitation energy $E_1$ of the neutral atom. It is shown in Sec. III B that the photodetachment cross section will, in fact, also have an infinite derivative at this threshold. Thus, if this is observed at some wavelength $\lambda_c$, the electron affinity EA is then related to $E_1$ and $\lambda_c$ by

$$\mathrm{EA} = (1/R\lambda_c) - E_1 , \tag{1.1}$$

where EA and $E_1$ are in rydbergs and $R$ is the rydberg constant for the particular species.

Assuming Weiss's values for the electron affinities, 0.0453 Ry for $Li^-$, 0.0396 Ry for $Na^-$, and 0.0347 Ry for $K^-$, and taking the values of $R$ to be 109728.64 $cm^{-1}$, 109734.69 $cm^{-1}$ and 109735.77 $cm^{-1}$, respectively, the $\lambda_c$ values are 5032, 4692, and 5941 Å, respectively. The electron affinities of the heavier alkali metals are assumed to be comparable, and hence photodetachment to the region near the first excitation threshold of all the neutral alkali metals is well within the capability of modern dye lasers operating in the visible. The suggestion[12] that this threshold behavior might be exploited in order to determine the electron affinities of the alkali metals by this method was very quickly confirmed[13] and affinities of $Na^-$, $K^-$, $Rb^-$, and $Cs^-$ have been measured[14] to much greater accuracy than previously.

The present work has several purposes: to obtain reliable photodetachment cross sections for $Li^-$, $Na^-$ and $K^-$ using some of the most accurate wave functions available, thereby also providing a test of simpler approximations[15-18]; and to study in some detail the structure of these cross sections near the first excitation threshold of the neutral atoms. The configuration-interaction wave functions of Weiss[5] are used for the initial state. For the final states we use the solutions of close-coupling equations for electron scattering by the neutral atoms. The calculation of these latter wave functions is discussed in Sec. II, along with the implications for photodetachment of the scattering results near the first excitation threshold. The way in which the photodetachment cross section is obtained, and the threshold behavior, is discussed in Sec. III. Photodetachment results are presented and discussed in Sec. IV.

## II. SCATTERING

The present work is based on a semiempirical calculation of the radial wave functions for the neutral atoms in which an effective potential is used to represent all interactions between the single valence electron and the nucleus and closed-shell electron core. The scattering calculation is then treated as a simple two-electron problem, and carried out using the coupled equations formalism in $LS$ coupling. Detailed calculations[11] for Na using this technique yielded results in good agreement with a variety of experimental measurements. These include differential[19,20] and total[21] scattering, excitation,[22,23] and the polarization of the resonance radiation following collisional excitation.[22]

### A. Target model

The equation for the radial part of the valence electron wave function is taken to be

$$\left( \frac{d^2}{dr^2} - \frac{l(l+1)}{r^2} + V(r) + \epsilon_{nl} \right) P_{nl}(r) = 0 , \tag{2.1}$$

where the model potential is composed of two terms,

$$V(r) = V(\lambda, r) + V_p(r) , \tag{2.2}$$

the first of which is the scaled Thomas-Fermi-Dirac statistical model potential[24] with limiting forms

$$\lim_{r\to 0} V(\lambda, r) \sim \frac{2Z}{r} , \quad \lim_{r\to\infty} V(\lambda, r) = \frac{2}{r} , \tag{2.3}$$

where $\lambda$ is an adjustable parameter and $Z$ is the nuclear charge. The polarization potential $V_p(r)$ represents the effect of induced-core moments on the valence electron and is taken to be

$$V_p(r) = \frac{\alpha_d}{r^4} W_6(r_c, r) + \frac{\alpha_q'}{r^6} W_{10}(r_c, r) , \tag{2.4}$$

where $\alpha_d$ and $\alpha_q'$ are the dipole and effective quadrupole core polarizabilities, respectively, and $W_m(r_c, r)$ is a function introduced to cut off $V_p(r)$ near the origin. The parameters $\lambda$ and cutoff radius $r_c$ are adjusted until calculated values of $\epsilon_{nl}$ for the lowest few terms are in good agreement with spectroscopic values.

The model parameters for Li and Na were taken from earlier work[25] in which the simple approximations $\alpha_q' = 0$ and

$$W_6(r_c, r) = (1 + r_c^2/r^2)^{-2} \tag{2.5}$$

were used. For $K$ we used the form

$$W_m(r_c, r) = 1 - e^{-(r/r_c)^m} . \quad (2.6)$$

The values of the various constants adopted are given in Table I, along with calculated and spectroscopic term values. It is seen that the cutoff radii are of order of the core radius, as expected, and that the $r^{-6}$ term in (2.4) is relatively unimportant.

### B. Scattering model

Consistent with the approximation of Sec. II A, the equations describing the electron-neutral scattering system are formally equivalent to those for scattering by neutral hydrogen[26] with the nuclear Coulomb potential replaced by $V(r)$. It will prove useful in what follows to present the wave function for the scattering system in some detail. It is convenient to work in the representation $\Gamma = (\gamma L S M_L M_S)$ in which the atomic and electronic angular momenta are coupled to give total angular-momentum quantum numbers $LM_L SM_S$, with $\gamma = a l_2$ representing the atomic state $a = n_1 l_1$, relative to which the electron momentum is $k_a$, and the orbital angular momentum $l_2$ of the scattered electron.

The total wave function can be written

$$\Psi_{a m_1 \mu_1 \mu_2}(\vec{\mathrm{X}}_1 \vec{\mathrm{X}}_2) = \sum_{l_2, m_2} \sum_{L, M_L} \sum_{S, M_S} i^{l_2} C^{l_1 l_2 L}_{m_1 m_2 M_L} \times C^{1/2\ 1/2 S}_{\mu_1 \mu_2 M_S} Y^*_{l_2 m_2}(\hat{k}_a) \Phi_\gamma(LSM_L M_S | \vec{\mathrm{X}}_1 \vec{\mathrm{X}}_2), \quad (2.7)$$

where $\vec{\mathrm{X}}_i$ represents all space and spin coordinates of electron $i$, $\mu_1$ and $\mu_2$ are the spin projection quantum numbers, the $C$'s are Clebsch-Gordan coefficients, and

$$\Phi_\gamma(LSM_L M_S | \vec{\mathrm{X}}_1 \vec{\mathrm{X}}_2) = \frac{A}{\sqrt{2}} \frac{i}{2} \sum_{\gamma'} \sum_{m_1', m_2'} \sum_{\mu_1', \mu_2'} C^{l_1' l_2' L}_{m_1' m_2' M_L} \times C^{1/2\ 1/2 S}_{\mu_1' \mu_2' M_S} \psi_{\gamma' m_1' \mu_1' m_2' \mu_2'}(\vec{\mathrm{X}}_1 \hat{r}_2 \sigma_2) \times \frac{1}{r_2} F^{LS}_{\gamma' \gamma}(r_2), \quad (2.8)$$

where $A$ is the operator which exchanges the coordinates $1 \leftrightarrow 2$. The function $\psi$ is a product of the atomic wave function, the radial part of which is a solution of (2.1), and the spin and angular parts of the scattered electron wave function. The radial functions $F^{LS}_{\gamma' \gamma}(r_2)$ have asymptotic form

$$F^{LS}_{\gamma' \gamma}(r_2) \underset{r_2 \to \infty}{\sim} k_{a'}^{-1/2} (e^{-i(k_{a'} r_2 - 1/2 l_2' \pi)} \delta_{\gamma' \gamma} - e^{i(k_{a'} r_2 - 1/2 l_2' \pi)} S^{LS}_{\gamma' \gamma}),$$
$$F^{LS}_{\gamma' \gamma}(r_2) \underset{r_2 \to 0}{\sim} 0 \quad (2.9)$$

where $\underline{S}$ is the scattering matrix, which is diagonal in $L$ and $S$ and independent of $M_L$ and $M_S$.

Application of the variational condition yields the coupled integrodifferential equations

$$\left( \frac{d^2}{dr^2} - \frac{l_2'(l_2'+1)}{r_2^2} + V(r_2) + k_{a'}^2 \right) F^{LS}_{\gamma' \gamma}(r_2) = \sum_{\gamma''} (V_{\gamma' \gamma''} + W_{\gamma' \gamma''}) F^{LS}_{\gamma'' \gamma}(r_2) \quad (2.10)$$

for (2.9), where $V(r_2)$ is given by (2.2), and $V_{\gamma' \gamma''}$ and $W_{\gamma' \gamma''}$ are the direct and exchange potential operators, respectively, resulting from the Coulomb interaction of the atomic and scattered electrons. Expressions for these operators can be found elsewhere.[27] We note that polarization of the core by the scattered electron and atomic electron individually has been included by the use of $V(r)$ in (2.1) and (2.10), but we have neglected the effect of the moments induced by one electron on the other, the so-called dielectric correction.[28] This has been shown to be a relatively small effect for the lighter alkali metals,[6] at least as applied to the calculation of electron affinities, but is becoming significant for $K$. The consequence of this will be discussed in Sec. IV.

In practice we obtain solutions $G^{LS}_{\gamma' \gamma}(r_2)$ of (2.10) which obey real reactance-matrix boundary conditions

$$G^{LS}_{\gamma' \gamma}(r_2) \underset{r_2 \to \infty}{\sim} k_{a'}^{-1/2} [\sin(k_{a'} r_2 - \tfrac{1}{2} l_2' \pi) \delta_{\gamma' \gamma} + \cos(k_{a'} r_2 - \tfrac{1}{2} l_2' \pi) R_{\gamma' \gamma}], \quad (2.11)$$
$$G^{LS}_{\gamma' \gamma}(r_2) \underset{r_2 \to 0}{\sim} 0 .$$

TABLE I. Parameters of the semiempirical model potential, and calculated (a) and spectroscopic (b) term values. The energies $\epsilon_{nl}$ are in Ry and $a_0$ is the Bohr radius.

| | | Li | Na | K |
|---|---|---|---|---|
| $\lambda$ | | 0.6583 | 0.8050 | 1.0717 |
| $r_c, a_0$ | | 0.4678 | 0.6977 | 2.9236 |
| $\alpha_d, a_0^3$ | | 0.1851 | 0.8840 | 5.4730 |
| $\alpha_q', a_0^5$ | | | | 0.4296 |
| $\epsilon_{n_0 s}$ | a | −0.396 32 | −0.377 72 | −0.319 05 |
| | b | −0.396 31 | −0.377 72 | −0.319 04 |
| $\epsilon_{n_0 p}$ | a | −0.260 49 | −0.223 10 | −0.200 34 |
| | b | −0.206 49 | −0.223 10 | −0.200 36 |
| $\epsilon_{n_1 s}$ | a | −0.148 55 | −0.143 41 | −0.127 64 |
| | b | −0.148 38 | −0.143 16 | −0.127 43 |
| $\epsilon_{3d}$ | a | −0.111 22 | −0.111 98 | −0.125 16 |
| | b | −0.111 22 | −0.111 88 | −0.122 79 |

These functions are linear combinations of the solutions $F_{\gamma}^{LS}{}_{i_\gamma}(r_2)$ such that

$$\underline{F}^{LS} = -2i\underline{G}^{LS}(1 - i\underline{R})^{-1}. \tag{2.12}$$

The reactance and scattering matrices R and $S$ are related by

$$\underline{S} = (1 + i\underline{R})(1 - i\underline{R})^{-1}, \tag{2.13}$$

and the scattering cross sections for initial state $a$ and final state $a'$ are given by

$$Q(a \to a') = \pi a_0^2 \sum_{LS} Q^{LS}(a \to a'), \tag{2.14}$$

where

$$Q^{LS}(a \to a') = \frac{(2L+1)(2S+1)}{4k_a^2} \sum_{\gamma\gamma'} |\delta_{\gamma\gamma'} - S_{\gamma\gamma'}|^2. \tag{2.15}$$

The sum over $\gamma'$ in (2.8), in principle, runs over all bound and continuum states of the neutral atom, implying that (2.10) is an infinite set of coupled equations. In practice the sum must be truncated after a small number of terms. In the present work we include up to four target states in the sum, the lowest two $s$ states and the lowest $p$ and $d$ states.

The phase shifts obtained for the $^1P^0$ partial wave are shown in Fig. 1. The effect of including various numbers of states in the expansion (2.8) was studied in some detail for Na. At $k_1^2 = 0.151$ Ry, for example, a three-state ($3s$, $3p$, $3d$) calculation led to an increase in the phase shift by 10% over a two-state ($3s, 3p$) calculation, but adding the $4s$ state in a four-state calculation led to a further increase of less than 1%. Comparable results were obtained in two- and three-state calculations in Li. Accordingly, we carried out all further work for all three species in the three-state ($n_0s$, $n_0p$, $3d$) approximation, except that below the energy where the two-state and three-state phase shifts agreed to 2% or better, the former were used. These transition points were 0.0588, 0.0955, and 0.0588 Ry in Li, Na, and K, respectively.

In all cases we note that the phase shift exhibits strongly resonant behavior below the first excitation threshold, but that only for K does the phase shift achieve $\frac{1}{2}\pi$ before the threshold is reached. The resonance might be labeled the $n_1sn_0p\ ^1P^0$ autoionizing state of the negative ion,[14] but too much significance should not be attached to this label. (There is also evidence that these states exist, and are more strongly bound, in $Rb^-$ and $Cs^-$.[14]) The existence of autoionizing states of $Li^-$ and $Na^-$ at even higher energies has also been suggested.[29]

### C. Threshold behavior

If it is assumed that the potentials $V_{\gamma'\gamma''}$ and $W_{\gamma'\gamma''}$ of Eq. (2.10) are of finite range, then the behavior of the cross sections in the neighborhood of an excitation threshold may be studied by applying many-channel effective range theory.[30] In this case, a matrix $\underline{M}$ may be defined which is a meromorphic function of the energy, whose elements vary sufficiently slowly as a function of energy that they may be regarded as constant for the purposes of obtaining threshold laws. $\underline{M}$ is related to the reactance matrix $\underline{R}$ by the equation

$$\underline{R} = \underline{k}^{l+1/2}\underline{M}^{-1}\underline{k}^{l+1/2}, \tag{2.16}$$

where $\underline{k}^{l+1/2}$ is a matrix with elements $k_i^{l_i+1/2}\delta_{ij}$. Substitution of (2.16) in (2.13) and (2.15) leads to expressions for the partial cross sections near thresholds, and the resulting behavior is a generalization of the Wigner threshold law[31] to the many-channel case. In practice, for electron-atom scattering, the potentials are not short range, in general behaving asymptotically as some inverse power of $r$. For hydrogenic targets, the long-range inverse square potential coupling channels

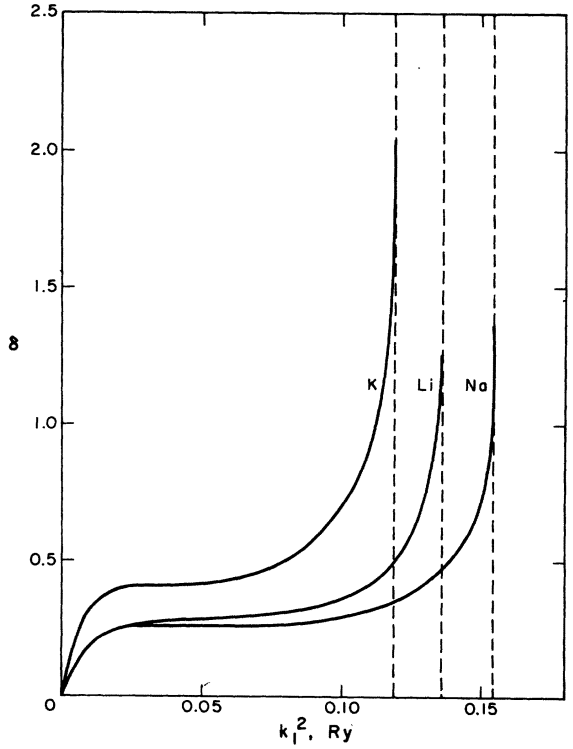


FIG. 1. Phase shifts for electron–alkali-metal-atom elastic scattering in the $^1P^0$ partial wave, calculated in the three-state ($n_0s$, $n_0p$, $3d$) close-coupling approximation.

belonging to degenerate target states leads to modifications of the threshold law.[32-34]

The case of interest in this paper is that of $^1P^0$ electron-alkali-metal scattering in the vicinity of the threshold for the first excited state, $n_0p$. In order to understand the threshold behavior of the partial cross sections, it suffices to consider a two-state ($n_0s$, $n_0p$) close-coupling formulation. We then have three channels, $\gamma_1 = n_0 s k_1 p$, $\gamma_2 = n_0 p k_2 s$, and $\gamma_3 = n_0 p k_2 d$, with $k_1^2 > k_2^2$. Below threshold $k_2 = i|k_2|$. At energies of interest, the effects of $\gamma_3$ can be neglected. The potentials $V_{11}$, $V_{22}$ and $W_{\gamma'\gamma''}$ fall off exponentially (except for an initial Coulomb term), and $V_{12}$ is proportional to $r^{-2}$ for large $r$. It has been shown[34] that in these circumstances, no modification of (2.16) is required. We obtain, therefore, from (2.13), (2.15), and (2.16), for small $|k_2|$ and $L=1$, $S=0$,

$$Q_{11} = Q_{11}(0)[1 - (2B/C)|k_2|] \tag{2.17}$$

for $k_2^2 \lesssim 0$, and

$$\begin{aligned} Q_{11} &= Q_{11}(0)(1 - 2Bk_2)\,, \\ Q_{12} &= (3B/k_1^2)k_2\,, \\ Q_{22} &= 3(A^2 + B^2)\,, \end{aligned} \tag{2.18}$$

for $k_2^2 \gtrsim 0$, where

$$Q_{11}(0) = 3C^2/k_1^2(1 + C^2)\,. \tag{2.19}$$

The constants $A$, $B$, and $C$ are given by

$$C = k_1^3 P_{11}\,, \quad B = k_1^3 P_{12}^2/(1 + C^2)\,, \quad A = BC - P_{22}\,, \tag{2.20}$$

where

$$\underline{P} = \underline{M}^{-1}\,. \tag{2.21}$$

Since $B > 0$, $Q_{11}$ is falling, and $Q_{12}$ rising, just above threshold. The elastic cross section thus has an infinite derivative with respect to $k_1^2$ at threshold, resulting in either a cusp ($C > 0$) or step ($C < 0$).

Results obtained for the $^1P^0$ partial cross sections, using a new algorithm developed for near-threshold electron-neutral scattering calculations,[35] yielded a cusp for Li and Na, but for K the elastic cross section takes the form of a step (Fig. 2). Values of the constants $B$ and $C$ at threshold for K were obtained by interpolation, and were used to give the straight lines in Fig. 2 representative of the threshold law. Simple interpolation was not possible for Li and Na, but it was found that the three partial cross sections obtained at $k_2^2 = \pm 10^{-5}$ Ry could not be adequately fitted by (2.17)–(2.19), for any choices of the two constants $B$ and $C$. Since the threshold law must be satisfied even by a model calculation such as the present one, its validity is obviously restricted to an extremely narrow energy range. The explanation is clearly that $P_{11}$ and $P_{12}$ are constant only to first order, and vary rapidly away from threshold, presumably due to resonant behavior introduced by the long-range potential $V_{12}$. We conclude that it is primarily a resonance, not the Wigner threshold law, which provides the structure in the $^1P^0$ partial scattering cross sections. This conclusion is supported by calculations for the $^3P^0$ partial wave,[9-11,34] in which resonant behavior is absent, and for which the Wigner threshold law has almost negligible effect on the partial scattering cross sections.

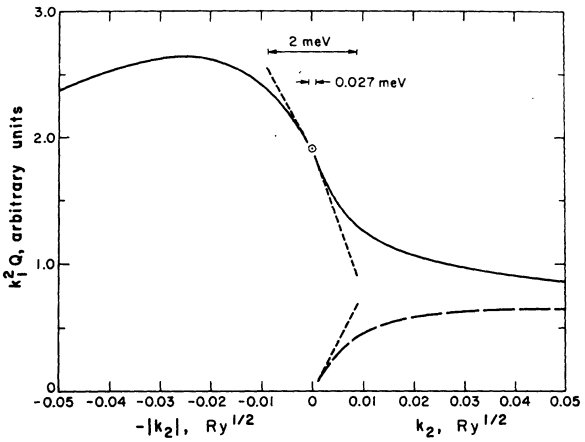


FIG. 2. Partial $^1P^0$ cross sections for elastic (solid line) and inelastic (long dashed line) electron-potassium scattering in the vicinity of the $4p$ threshold. The short dashed lines are the cross sections given by the Wigner threshold law.

## III. PHOTODETACHMENT

We consider photodetachment of an alkali-metal negative ion by photons with polarization $\hat{n}$, the electron being ejected with wave vector $\vec{k}_a$, and the neutral atom being left in the final state $a$. For photon energy $E_\nu$,

$$E_\nu = \mathrm{EA} + k_a^2 + E_a\,, \tag{3.1}$$

where EA is the electron affinity, $E_a$ is the excitation energy of state $a$, and $k_a^2$ is the ejected electron energy.

### A. Photodetachment model

If we neglect all transitions of inner-shell electrons, we are dealing with a two-electron system, and the partial differential photodetachment cross section can be expressed in dipole length form

$$\frac{dK^{(L)}}{d\vec{k}_a}(\vec{k}_a) = \frac{4\pi\alpha a_0^2 E_\nu}{\omega_i} \sum \left| \int \Psi_f^* \hat{n} \cdot (\vec{r}_1 + \vec{r}_2) \Psi_i \, d\tau \right|^2\,, \tag{3.2}$$

and in dipole velocity form

$$\frac{dK^{(V)}}{d\hat{k}_a}(\vec{k}_a)=\frac{16\pi\alpha a_0^2}{\omega_i E_\nu}\sum\left|\int\Psi_f^*\hat{n}\cdot(\vec{\nabla}_1+\vec{\nabla}_2)\Psi_i\,d\tau\right|^2. \tag{3.3}$$

Here $\alpha$ is the fine-structure constant, $a_0$ is the Bohr radius, $\omega_i$ is the statistical weight of the initial state, and the summation runs over all degenerate initial and final states. The initial-state wave function is $\Psi_i$, assumed unit normalized, and $\Psi_f$ is the final-state atom-plus-electron wave function, with normalization

$$\int\Psi_f^*(\vec{k}_a)\Psi_f(\vec{k}_a')\,d\tau=\tfrac{1}{2}\pi k_a\delta(\vec{k}_a-\vec{k}_a'). \tag{3.4}$$

The length and velocity cross sections should be equal in the limit of exact wave functions, but since we will of necessity be using approximate wave functions, comparison of length and velocity results provides a check on the accuracy of the model.

In the present work we take the results of Weiss[5] for the initial states, which are a superposition of configurations $\alpha=n_1'l_1'n_2'l_2'$ of the form

$$\Psi_i(L'S'M_L'M_S'\,|\,\vec{x}_1\vec{x}_2)=\sum_\alpha A_\alpha\Phi_\alpha(L'S'M_L'M_S'\,|\,\vec{x}_1\vec{x}_2), \tag{3.5}$$

where the $\Phi_\alpha$ are antisymmetric with respect to interchange of space and spin coordinates, and the $A_\alpha$ are the configuration-interaction coefficients. To illustrate the importance of configuration interaction in these calculations, we give in Table II the configuration-interaction coefficients of the six most important configurations (of 14, 11, and 9 for $Li^-$, $Na^-$, and $K^-$, respectively). Consistent with the scattering model, we take only the two outer electrons of the negative ion into account.

TABLE II. Configuration-interaction coefficients of the first six configurations in the negative-ion wave functions of Weiss.[5]

| $Li^-$ | | $Na^-$ | | $K^-$ | |
|---|---|---|---|---|---|
| $2s^2$ | 0.931 | $3s^2$ | 0.941 | $4s^2$ | 0.935 |
| $2p^{2\,a}$ | 0.330 | $3p^{2\,a}$ | 0.305 | $4p^{2\,a}$ | 0.334 |
| $3d^2$ | −0.012 | $3d^2$ | −0.017 | $3d^2$ | −0.018 |
| $3s^2$ | −0.111 | $4s^2$ | −0.118 | $5s^2$ | −0.109 |
| $2s3s$ | −0.095 | $3s4s$ | 0.074 | $4s5s$ | −0.053 |
| $2s4s$ | 0.048 | $3s5s$ | 0.038 | $4s6s$ | −0.007 |

[a]The signs of the $p^2$ configurations have been changed to correspond to the phase convention used in the present work.

The coupled scattering wave functions given by (2.7) are used for the final state $\Psi_f$. The form of (2.7)–(2.9) was chosen so as to satisfy the normalization condition (3.4). This function, however, has the outgoing wave form, $\Psi_f^{(+)}$, whereas it is well known that the incoming wave form, $\Psi_f^{(-)}$, should be used in calculations of this type. It is easily shown that $[\Psi_f^{(-)}]^*$ is simply the function given by (2.7)–(2.9) with the factor $i^{l_2}$ replaced by $(-i)^{l_2}$, and hence we may write (3.2) as

$$\frac{dK^{(L)}(\vec{k}_a)}{d\hat{k}_a}=\frac{4\pi\alpha a_0^2E_\nu}{(2L'+1)(2S'+1)}\sum_{M_L',M_S'}\sum_{m_1,\mu_1,\mu_2}\Bigg|\sum_{l_2,m_2}\sum_{L,S}\sum_{M_L,M_S}(-i)^{l_2}Y_{l_2m_2}^*(\hat{k}_a)$$
$$\times C^{l_1l_2L}_{m_1m_2M_L}C^{1/2\,1/2\,S}_{\mu_1\mu_2M_S}\langle al_2LSM_LM_S\,|\,\hat{n}\cdot(\vec{r}_1+\vec{r}_2)\,|\,L'S'M_L'M_S'\rangle\Bigg|^2, \tag{3.6}$$

where the primed and unprimed quantities refer to the initial and final states, respectively, and the matrix element involves the wave functions given by (2.8) and (3.5).

Integrating over all angles of the ejected electron and averaging over all polarizations of the light we obtain the partial cross section

$$K^{(L)}(k_a)=\frac{4\pi\alpha a_0^2E_\nu}{(2L'+1)}\sum_{l_2L}|M^{(L)}(al_2LL'S')|^2 \tag{3.7}$$

in terms of the reduced matrix elements

$$M^{(L)}(al_2LL'S')=\langle al_2LS'\,||\,z_1+z_2\,||\,L'S'\rangle. \tag{3.8}$$

Two special cases of (3.6) are of interest. For light polarized linearly along the $z$ axis ($\hat{n}\cdot\hat{z}=1$)

$$\frac{dK^{(L)}(\vec{k}_a)}{d\hat{k}_a}=\frac{K^{(L)}(k_a)}{4\pi}[1+\beta^{(L)}(k_a)\tfrac{1}{2}(3\cos^2\theta-1)], \tag{3.9}$$

and for unpolarized light incident along the $z$ axis ($\hat{n}\cdot\hat{z}=0$) the form is as (3.9) with $\beta$ replaced by $-\frac{1}{2}\beta$. In (3.9) $\cos\theta=\hat{k}_a\cdot\hat{z}$, and $\beta$ is known as the asymmetry parameter, given by[36]

$$\beta^{(L)}(k_a)=\left(3(-1)^{l_1+L'}\Big/\sum_{l_2L}\left|M^{(L)}(al_2LL'S')\right|^2\right)\sum_{l_2,l_2''}\sum_{L,L''}i^{l_2-l_2''}[(2l_2+1)(2l_2''+1)(2L+1)(2L''+1)]^{1/2}$$
$$\times C^{l_2l_2''2}_{000}C^{112}_{000}W(l_2l_2''LL'',2l_1)W(11LL'',2L')M^{(L)}(al_2LL'S')M^{(L)*}(al_2''L''L'S'), \tag{3.10}$$

where the $W$'s are Racah coefficients.

For alkali-metal negative ions initially in the ground state $L' = S' = 0$, implying that $L = L'' = 1$. If the photodetachment process leaves the neutral alkali-metal atom in the ground $(n_0 s)$ state, $l_2 = 1$, we obtain the result $\beta^{(L)}(k_{n_0 s}) \equiv 2$. For linearly polarized light, therefore, the differential cross section vanishes in the plane normal to the direction of polarization, while for unpolarized light the differential cross section vanishes in the direction of light propagation, in accord with conclusions based on conservation of angular momentum. This is a relatively trivial result, but it should be noted that measurement of $\beta(k_{n_0 s})$ would provide a useful check on the assumption that photodetachment of the alkali-metal negative ions can be adequately represented in $LS$ coupling, with neglect of the spin-orbit interaction.

For photon energies sufficient to leave the neutral atom in the first excited state $(n_0 p)$ we obtain

$$\beta^{(L)}(k_{n_0 p}) = \frac{|M_2^{(L)}|^2 + \sqrt{2}\,(M_0^{(L)} M_2^{(L)*} + M_2^{(L)} M_0^{(L)*})}{|M_0^{(L)}|^2 + |M_2^{(L)}|^2}\,, \tag{3.11}$$

where we use the shorthand notation $M_{l_2}$. Starting from (3.3) instead of (3.2), equations analogous to (3.6)–(3.11) can be derived for the dipole velocity form of the cross sections.

It is perhaps worth noting that if the formally incorrect outgoing wave form $\Psi_f^{(+)}$ were used instead of $\Psi_f^{(-)}$ in the previous development, the results (3.6)–(3.11) would be identical in every respect, except that $M$ would be replaced by $M^*$, and the converse. Since the first Clebsch-Gordan coefficient in (3.10) implies that $l_2 - l_2''$ is even, it follows that identical results for $K(k_a)$ and $\beta$ will be obtained with $\Psi_f^{(-)}$ and $\Psi_f^{(+)}$, even in the most general case of configuration interaction in the initial state and $L' > 0$.

The total cross section, in the present notation, is given by

$$K(E_\nu) = \sum_a K(k_a)\,. \tag{3.12}$$

In theory, the sum over $a$ should be over all possible states that can be excited at the energy $E_\nu$, including the continuum if $E_\nu$ is sufficiently large (double detachment); in practice it is limited, at all energies, to the number of states included in the close-coupling expansion. Thus, contributions from highly excited states, core electrons, and double detachment are not allowed for in this work.

As a check on the calculations, in addition to the comparison of length and velocity cross sections, the continuum oscillator strength sum[37]

$$N_0 = \frac{R^{-1}}{4\pi^2 \alpha a_0^2} \int_0^{\lambda_0} \frac{K\,d\lambda}{\lambda^2} \tag{3.13}$$

$\lambda_0$ being the threshold wavelength, may be computed. If there is only one bound state of the ion below the photodetachment threshold, $N_0$ should be very nearly equal to 2 if the wave functions are sufficiently accurate. Since the close-coupling expansion is limited to a finite number of terms, the neglected effects discussed in the preceding paragraph should tend to make the calculated $N_0$ somewhat less than 2. We may also evaluate[37]

$$\alpha_p = \frac{R}{\pi^2 \alpha a_0^2} \int_0^{\lambda_0} K\,d\lambda\,, \tag{3.14}$$

the dipole polarizability (in atomic units, $a_0^3$) of the outer electrons.

To facilitate the application of the results we will also obtain the radiative attachment coefficient for electrons with a Maxwellian velocity distribution at temperature $T$. This related to the total photodetachment cross section (assuming a Boltzmann distribution of atomic states) by

$$\mathcal{R}(T) = \left(\frac{2}{\pi}\right)^{1/2} \frac{g_i}{g_a} \frac{h^3 c}{(mkT)^{3/2}}\, e^{hc/\lambda_0 kT} \int_0^{\lambda_0} \frac{K}{\lambda^4} f(\lambda, T)\,d\lambda\,, \tag{3.15}$$

where

$$f(\lambda, T) = e^{-hc/\lambda kT}/(1 - e^{-hc/\lambda kT})\,, \tag{3.16}$$

$g_i$ and $g_a$ are the statistical weights of the ion and ground-state atom, respectively, and the constants $m$, $h$, $c$, and $k$ have their usual meaning.

### B. Threshold behavior

In order to investigate the threshold behavior of the photodetachment cross section we use a form of the many-channel quantum defect theory appropriate for collisions with neutral atoms.[38] This theory is essentially equivalent to the many-channel effective-range theory,[30] and applies for potentials having a finite range. In summary, one considers solutions $\underline{F}(\underline{P}|r)$, zero at the origin, which, outside the range of the potential, take the form

$$\underline{F}(\underline{P}|r) = f(r) + g(r)\underline{P}(E) \tag{3.17}$$

for $r \geq r_0$. The functions $f(r)$ and $g(r)$ are analytic in the energy, and the matrix $\underline{P}$ is given by (2.21). Writing the functions (2.9) symbolically as $\underline{F}(\underline{S}|r)$, one finds that

$$\underline{F}(\underline{S}|r) = -2i\underline{F}(\underline{P}|r)\underline{X}\,, \tag{3.18}$$

where

$$\underline{X} = \underline{k}^{l+1/2}(1 - i\underline{R})^{-1}. \tag{3.19}$$

Suppose we have $n$ channels, $n_0$ of which are open. We form a $n \times n_0$ rectangular matrix, $\underline{X}_0$, from the open-open and closed-open elements of $\underline{X}$; the physically meaningful solution of the scat-

tering problem can then be written in the form of an $n \times n_0$ matrix

$$\underline{F}_0(\underline{S}|r) = -2i\underline{F}(\underline{P}|r)\underline{X}_0 . \tag{3.20}$$

The photodetachment cross section is proportional to $\vec{\sigma}(\underline{S})\vec{\sigma}^{\dagger}(\underline{S})$, where $\vec{\sigma}(\underline{S})$ is the dipole matrix element

$$\vec{\sigma}(\underline{S}) = \langle \Psi_i | \mathcal{R} | \psi(\underline{S}) \rangle , \tag{3.21}$$

which can be expressed as a row vector with elements $\sigma_j(\underline{S})$, $j = 1$ to $n_0$. From (3.20) one obtains

$$\vec{\sigma}(\underline{S}) = -2i\vec{\sigma}(\underline{P})\underline{X}_0, \tag{3.22}$$

where $\vec{\sigma}(\underline{P})$ is a $1 \times n$ row vector whose elements are formed from the dipole matrix element of $\Psi(\underline{P})$. The reason for expressing $\vec{\sigma}(\underline{S})$ in this form is that $\vec{\sigma}(\underline{P})$ is analytic and slowly varying in energy; all the energy variation is contained in $\underline{X}_0$. The cross section is then proportional to

$$\vec{\sigma}(\underline{S})\vec{\sigma}^{\dagger}(\underline{S}) = \sum_{j=1}^{n_0} \sum_{i,k=1}^{n} \sigma_i(\underline{P}) X_{0ij} X^*_{0kj} \sigma^*_k(\underline{P}) . \tag{3.23}$$

This expression allows us to determine the energy variation of the cross section. In the general case, this involves a good deal of complicated matrix theory, and in the present paper we consider a particular case, that one discussed in Sec. II C. Here we have two channels, with $k_1^2 > 0$, $l_1 = 1$, $l_2 = 0$, and we are concerned with the region $|k_2| \simeq 0$. Below threshold $k_2 = i|k_2|$. Using (2.21) and (3.19)–(3.23) we obtain after some algebra

$$K(n_0 s) = K(0)(1 + C_1|k_2|) , \tag{3.24}$$

for $k_2^2 \lesssim 0$, and

$$\begin{aligned} K(n_0 s) &= K(0)(1 - C_2 k_2) , \\ K(n_0 p) &= C_3 k_2 , \end{aligned} \tag{3.25}$$

for $k_2^2 \gtrsim 0$. $C_1$, $C_2$, and $C_3$ are constant to first order, but depend in a complicated manner on $k_1$, $\sigma_1(\underline{P})$, $\sigma_2(\underline{P})$, and $\underline{P}$, and $K(0)$ is the threshold value. It can be shown that the sign of $C_1$ is undetermined *a priori* while $C_2$ and $C_3$ are both positive at threshold. The sign of the derivative of the total cross section, $K(n_0 s) + K(n_0 p)$, with respect to $k_1^2$ just above threshold is also undetermined *a priori*, but it is clearly infinite [barring the very unlikely eventuality that $K(0)C_2 = C_3$].

## IV. RESULTS AND DISCUSSION

The photodetachment cross sections obtained using the formulas given in Sec. III A are shown in Figs. 3–5. Theoretical values[5] of EA were used in (3.1), and the corresponding values of $E_v$ used throughout the calculations. A sharp upward cusp is obtained for both $Li^-$ and $Na^-$, while for $K^-$ the cross section at the neutral excitation threshold appears as a step. The length and velocity results are in reasonable agreement for $Li^-$ and $Na^-$, but not so satisfactory for $K^-$, particularly in this threshold region.

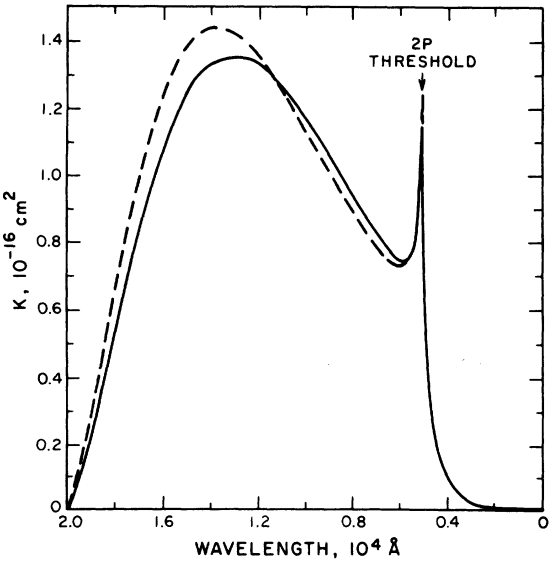


FIG. 3. Photodetachment cross section for $Li^-$, from the dipole length (dashed line) and dipole velocity (solid line) calculations.

The calculation of Moskvin[15] employed Hartree-Fock wave functions without configuration interaction for the negative-ion ground state, and plane waves for the continuum states. These results for $Li^-$, $Na^-$, and $K^-$ are larger than the present re-

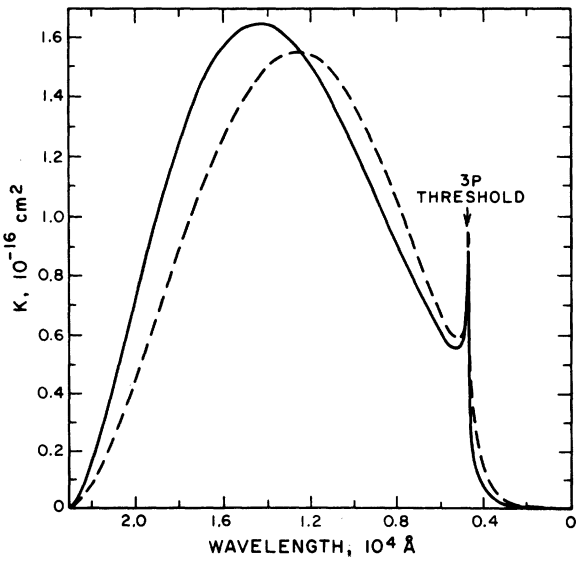


FIG. 4. Same as Fig. 3 for $Na^-$.

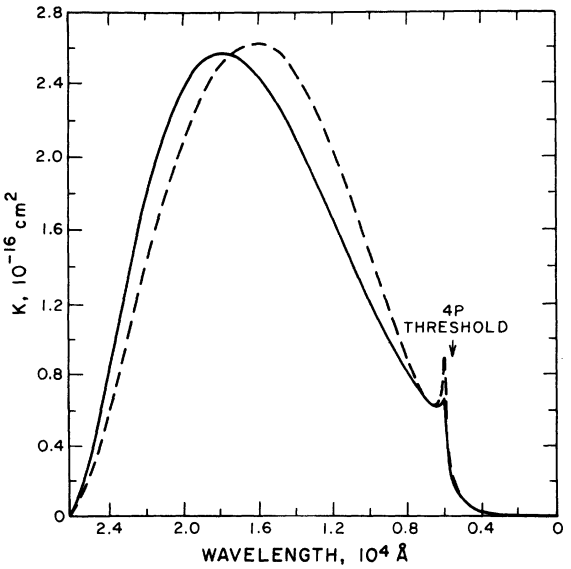


FIG. 5. Same as Fig. 3 for $K^-$.

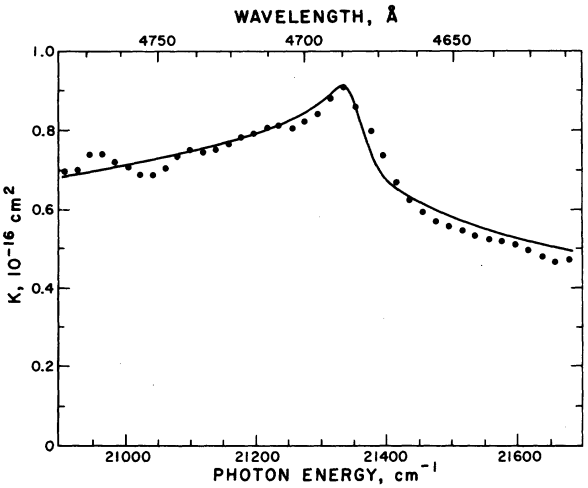


FIG. 6. Photodetachment cross section for $Na^-$ in the vicinity of the $3p$ threshold from the dipole length calculation and normalized experimental data (●) (Ref. 41). The theoretical results have been folded with the experimental resolution, and the experimental energy scale is used.

sults at the maxima by 50% or more, but the locations of the maxima are in reasonable agreement. The calculation of Ya'akobi[16] for $Li^-$ employed a simple semiempirical model potential approach suggested by Geltman,[39] yielding a cross section with a maximum about one-half as large as the present results, and at about twice the ejected electron energy. The calculation of John and Williams[17] employed the so-called Bethe-Longmire method,[40] which requires the specification of electron affinities (taken from Weiss[5]) and elastic electron-neutral phase shifts (taken from Karule[9]), and enforcement of the value $N_0 = 2$. The maxima in these results occur at significantly lower ejected electron energies than the present results for $Na^-$ and $K^-$, and are about one-half the present results in magnitude for $Li^-$ and $K^-$, but in reasonable agreement for $Na^-$. The calculations of McGinn[18] for $Li^-$ used a pseudopotential modification of the Hartree-Fock core potential to obtain the wave functions for $Li^-$, and a frozen core Hartree-Fock calculation for the continuum states. The cross section obtained has a maximum about 60% of the present result, located at a slightly higher ejected electron energy.

In Fig. 6 are shown, on a larger scale, the experimental results[41] for $Na^-$, obtained using a tunable dye laser. The shape of the measured curve in the region of the cusp is in excellent agreement with the present result, the peak being observed at 4687(±7) Å, compared with the Weiss value of 4692 Å. Also shown in Fig. 6 are the present dipole length results folded with the experimental wavelength resolution, and normalized in energy to make the peaks coincide. The experimental data, which are not absolute, have been normalized in turn to the theoretical results at about 4725 Å. This double normalization results in a good fit between the two curves (the fit using the dipole velocity results is even better) and leads to the conclusion that the experimentally observed feature is indeed the $3p$ threshold. The electron affinity of Na is then deduced, using (1.1), to be 0.543 (±0.010) eV.[14]

In Fig. 7 we show the results obtained for $K^-$ in the vicinity of threshold, together with experimental results.[41] The shape of the experiment is in good agreement with the dipole velocity results, but not with the dipole length results. The same normalization procedure (of the dipole velocity calculation) was adopted as in Fig. 6. Additional structure is observed in the experimental results at the center of the step, which is presumably the effect of the splitting of the $4p$ state into the $j = \frac{1}{2}$ and $j = \frac{3}{2}$ components. The present calculations do not include the spin-orbit interaction, and hence no such structure is obtained. Assuming that the first minimum represents the $4p_{1/2}$ threshold, an affinity of 0.5012 (±.0015) eV[14] is obtained for K compared with the value 0.472 eV of Weiss.[5]

The partial $K^-$ photodetachment cross sections are plotted against electron momentum relative to the $4p$ state in Fig. 8, over the same range of momentum as the partial scattering cross sections, Fig. 2. The partial cross section for the $4pk_2d$ channel, not shown, is more than two orders of magnitude less than that for the $4pk_2s$ channel.

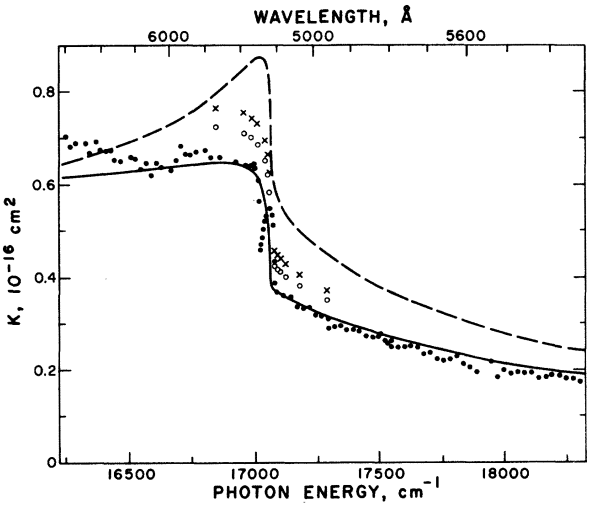


FIG. 7. Photodetachment cross section for $K^-$ in the vicinity of the $4p$ threshold from the dipole length (dashed line) and dipole velocity (solid line) calculations and normalized experimental data (●) (Ref. 41). Dipole length and velocity results obtained using a close-coupling wave function for the negative ion are given by (○) and (×), respectively. The experimental energy scale is used.

We see that, like the partial cross sections for electron scattering, the partial cross sections for photodetachment depart from the linear behavior demanded by the threshold law (3.24) and (3.25), for very small energies relative to the $4p$ threshold.

The asymmetry parameters $\beta(k_2)$ for the slow photoelectrons above the threshold are plotted in Fig. 9. The results are clearly sensitive to the

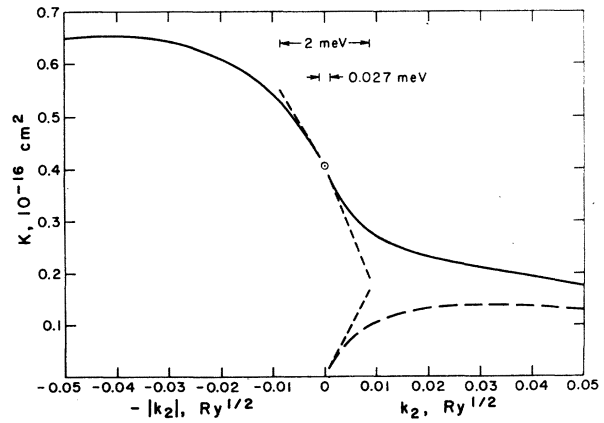


FIG. 8. Partial photodetachment cross sections for $K^-$ in the vicinity of the $4p$ threshold from the dipole velocity calculation, for the $4sk_2p$ (solid line) and $4pk_2s$ (long dashed line) channels. The short dashed lines are the cross sections given by the Wigner threshold law.

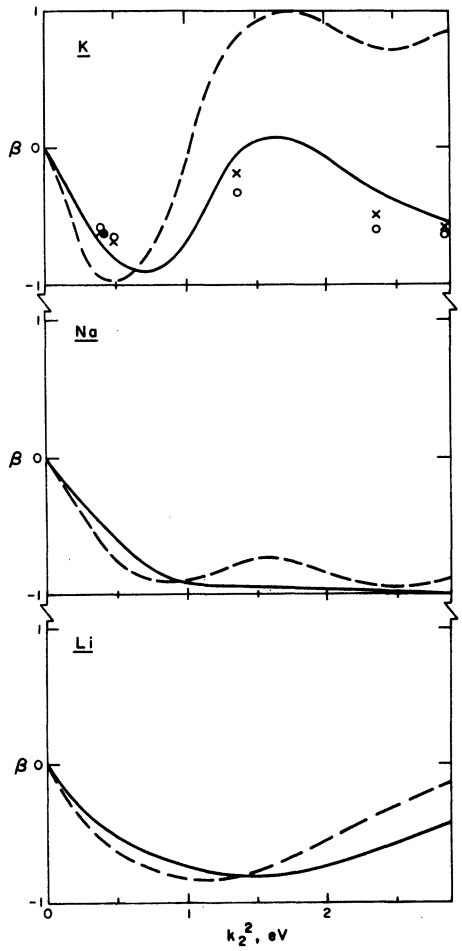


FIG. 9. Angular distribution parameter $\beta$ for photoelectrons from the first excited state of Li, Na, and K following photodetachment, from the dipole length (dashed line) and dipole velocity (solid line) calculations, and experimental result (●) (Ref. 42) for $K^-$. Results of improved dipole length and velocity calculations for $K^-$ are given as (○) and (×), respectively.

choice of dipole operator, but for $Li^-$ and $Na^-$ the length and velocity results are still in reasonable agreement. For $K^-$ however, very large differences are obtained above 1.0 eV. The experimental value[42] at 0.425 eV is in better agreement with the velocity calculation.

Values obtained for $N_0$ are given in Table III. It might be noted that use of measured[14] rather than theoretical[5] values of EA in (3.1), and therefore (3.6), would lead to a slightly larger value of $N_0^{(L)}$ and slightly smaller value of $N_0^{(V)}$, and that the results most affected would be those for $K^-$. The results for $Li^-$ and $Na^-$ are little changed from the earlier two-state results,[12] since the dominant contribution to $N_0$ comes from the long-wavelength region, where the addition of higher states in the

TABLE III. Values of the oscillator density integral $N_0$, dipole polarizability $\alpha_p$ [a] (in units of $a_0^3$), and $\chi_0$ (in units of $a_0^2$). The contribution to the total from the inelastic region is given in parentheses, in %.

| | $Li^-$ | $Na^-$ | $K^-$ |
|---|---|---|---|
| $N_0^{(L)}$ | 1.94(18) | 2.04(10) | 2.22(7.3) |
| $N_0^{(V)}$ | 1.90(16) | 1.90(6.2) | 1.99(6.2) |
| $\alpha_p^{(L)}$ | 832(2.6) | 989(1.6) | 1805(0.9) |
| $\alpha_p^{(V)}$ | 798(2.6) | 1058(0.8) | 1757(0.7) |
| $\chi_0^{(L)}$ | 54.3 | 61.8 | 88.3 |
| $\chi_0^{(V)}$ | 53.0 | 61.8 | 82.3 |

[a] The total negative-ion polarizability is the sum of this quantity and the values $\alpha_d$ of Table I.

expansion (2.8) has little effect on the cross section. The dipole polarizabilities of the negative ions, also given in Table III, were changed even less for the same reason. In view of the magnitude of the contribution to $N_0$ from the inelastic region, i.e., that above the first excitation threshold of the neutral atom, where we expect the calculation to underestimate the total cross section, the dipole velocity results appear to agree better with the correct result of 2.00.

We note that in addition to (3.13) and (3.14) a third sum rule follows from the application of closure,[37] viz.,

$$\int \Psi_f^*(\vec{r}_1+\vec{r}_2)^2\Psi_i\, d\tau = \frac{3}{4\pi^2\alpha a_0^2}\int_0^{\lambda_0}\frac{K}{\lambda}\,d\lambda . \qquad (4.1)$$

Evaluation of the right-hand-side of (4.1) yielded the results labeled $\chi_0$ in Table III. Values for the left-hand-side of (4.1) have been obtained from the negative-ion wave functions used in the present work, and from preliminary calculations using the wave functions of Ref. 6 (row b, Table I of that work). The results are 54.5, 62.0, and 89.5 from the former, and 53.0, 62.2, and 78.9 from the latter, for $Li^-$, $Na^-$ and $K^-$, respectively.

The radiative attachment coefficient (3.15) has been evaluated for $K^{(V)}$, and fitted for $T$ between 200 and 20 000°K to the expression

$$\mathcal{R}(T) = \tfrac{1}{2}[b_0(T) - b_2(T)] , \qquad (4.2)$$

where $b_0(T)$ and $b_2(T)$ are obtained recursively from

$$b_n(T) = a_n + 2b_{n+1}(T)\log_{10}(\tfrac{1}{2}T) - b_{n+2}(T) , \qquad (4.3)$$

starting with $b_{n+1} = b_{n+2} = 0$. The constants in (4.3) are given in Table IV, yielding $\mathcal{R}(T)$ in units of $10^{-15}$ cm$^3$ sec$^{-1}$ for $T$ in °K to an accuracy of better than 2%.

All of the evidence indicates that the wave functions used in the $K^-$ calculations are less accurate than those used in the other cases, the inaccuracy being such that the length results are more affected than the velocity results. This suggests that the inaccuracy could lie in the long-range part of one or both of the sets of wave functions used. In model potential calculations such as this, there is no *a priori* reason to favor either length or velocity results, but given the manner in which the initial-state wave functions were obtained, there are reasons to believe that the velocity results might be preferable in this particular case.[12] Considering the final state, errors could arise either in the target atom functions, which are probably less accurate in K (see Table I) or in the scattered electron wave functions. The latter possibility could arise if insufficient states were included in the close-coupling expression. The discrepancies are not confined, however, to energies for which coupling to higher states is liable to be important. The omission of the so-called dielectric term,[6] mentioned in Sec. II B, could be more significant for the dipole length calculations, since it is a long-range interaction.

We have done some preliminary calculations using the wave functions from Ref. 6 for the ground state. This has the advantage that the same approximation is now used for both the initial and final state. It should be pointed out that this does *not* mean that dipole and velocity matrix elements should be identical. For inexact wave functions, a necessary condition for identity of the two matrix elements is that the dipole length operator commute with the Hamiltonian. This is not the case in the present calculation owing to the presence of the exchange operator in (2.10). Good agreement between the length and velocity results remains, therefore, a necessary but not sufficient condition for the validity of the results.

The results of these calculations for $K^-$ are included in Figs. 7 and 9. The same number of states were included in the expansion (2.8) as in the earlier calculations, but the improvement is quite marked. It is interesting to note that the velocity results are changed less than the length

TABLE IV. Constants to be used in the Chebeyshev expansion for the radiative attachment coefficient.

| | $Li^-$ | $Na^-$ | $K^-$ |
|---|---|---|---|
| $a_0$ | 8.741 34 | 8.427 41 | 9.895 61 |
| $a_1$ | 3.218 68 | 3.107 57 | 2.106 11 |
| $a_2$ | −0.507 815 | −0.584 271 | −1.386 41 |
| $a_3$ | −0.439 885 | −0.496 106 | −0.319 230 |
| $a_4$ | −0.076 930 9 | −0.052 137 0 | 0.097 717 0 |
| $a_5$ | −0.022 858 1 | | |

results and that the two sets of results are now in much better agreement with each other. The shape of both sets of results is now in good agreement with the experimental observation. The improvement is even more striking in the case of the asymmetry parameter $\beta$. The results of the length and velocity calculations agree to within 2% near 0.5 eV and are both within the uncertainty of the measured value, $0.64 \pm 0.02$,[42] at 4880 Å. At higher energies the large discrepancy between the length and velocity results is removed, and the new results are in much better agreement with the old dipole velocity results, as expected.

In future papers further results using this new model will be presented. The calculations will be extended to the heavier ions $Rb^-$ and $Cs^-$, for which experimental results have recently been obtained.[14,41,42] The fine-structure splitting of the $^2P$ excited state of these neutral atoms is even larger, and some fascinating structure has been observed at these thresholds.[41] It is hoped that we will be able to gain some increased understanding of this structure by including the spin-orbit interaction in the photodetachment calculation.

## ACKNOWLEDGMENTS

We would like to thank the authors of Refs. 38 and 41 for permission to quote their results in advance of publication, and Mrs. C. Kunasz for carrying out the computer fitting that led to the results given in Tables III and IV.

---

†This work was supported in part by National Science Foundation, Grant No. GP-39308X.

*Visiting Fellow, 1971–1972. Present address: Department of Physics and Astronomy, University College London, Gower Street, London WC1E-6BT, England, United Kingdom.

[1]B. L. Moiseiwitsch, Adv. At. Mol. Phys. 1, 61 (1965).
[2]B. M. Smirnov, Teplofiz. Vys. Temp. 3, 775 (1965) [Sov. Phys.-High Temp. 3, 716 1965].
[3]B. Steiner, in *Case Studies in Atomic Collision Physics*, edited by E. W. McDaniel and M. R. McDowell (North-Holland, Amsterdam, 1972), Vol. II, p. 483.
[4]J. N. Bardsley, Case Studies in Atomic Collision Physics (to be published).
[5]A. W. Weiss, Phys. Rev. 166, 70 (1968).
[6]D. W. Norcross, Phys. Rev. Lett. 32, 192 (1974).
[7]S. J. Smith and L. M. Branscomb, Rev. Sci. Instrum. 31, 733 (1960).
[8]W. C. Lineberger and B. W. Woodward, Phys. Rev. Lett. 25, 424 (1970).
[9]F. M. Karule, JILA Information Center Report No. 3, University of Colorado, Boulder (unpublished) [translation of *Atomic Collisions III*, edited by Y. Ia Veldre (Latvian Academy of Sciences, Riga, 1965)].
[10]P. M. Burke and A. J. Taylor, J. Phys. B 2, 869 (1969).
[11]D. L. Moores and D. W. Norcross, J. Phys. B 5, 1482 (1972). Dr. I. Hertel has kindly pointed out an error in this paper. The sentence following Eq. (2.12) should read, "For $|M|=1$ we have $f^{\pm}_{-1} = -f^{\pm}_{1}$."
[12]D. W. Norcross and D. L. Moores, in *Atomic Physics 3*, edited by S. J. Smith and G. K. Walters (Plenum, New York, 1973), p. 261.
[13]H. Hotop, T. A. Patterson, and W. C. Lineberger, Bull. Am. Phys. Soc. 17, 1128 (1972).
[14]T. A. Patterson, H. Hotop, A. Kasdan, D. W. Norcross, and W. C. Lineberger, Phys. Rev. Lett. 32, 189 (1974).
[15]Yu. V. Moskvin, Teplofiz. Vys. Temp. 3, 821 (1965) [Sov. Phys-High Temp. 3, 765 (1965)].
[16]B. Ya'akobi, Phys. Rev. 184, 246 (1969).
[17]T. L. John and A. R. Williams, J. Phys. B 5, 1662 (1972).
[18]G. McGinn, J. Chem. Phys. 54, 1671 (1971).
[19]D. Andrick, M. Eyb, and H. Hofmann, J. Phys. B 5, L15 (1972); private communication.
[20]W. Gehenn and E. Reichert, Z. Phys. 254, 28 (1972).
[21]A. Kasdan, T. M. Miller, and B. Bederson, Phys. Rev. A 8, 1562 (1973).
[22]E. A. Enemark and A. Gallagher, Phys. Rev. A 6, 192 (1972).
[23]H. Hafner, Phys. Lett. A 43, 275 (1973).
[24]W. Eissner and H. Nussbaumer, J. Phys. B 2, 1028 (1969).
[25]D. W. Norcross, J. Phys. B 4, 1458 (1971).
[26]I. C. Percival and M. J. Seaton, Proc. Camb. Philos. Soc. 53, 654 (1957).
[27]A. Salmona and M. J. Seaton, Proc. Phys. Soc. 77, 617 (1961).
[28]C. D. H. Chisholm and U. Öpik, Proc. Phys. Soc. 83, 541 (1964).
[29]A. C. Fung and J. J. Matese, Phys. Rev. A 5, 22 (1972).
[30]M. H. Ross and G. L. Shaw, Ann. Phys. (N. Y.) 13, 147 (1961).
[31]E. P. Wigner, Phys. Rev. 73, 1002 (1949).
[32]M. Gailitis and R. Damburg, Proc. Phys. Soc. 82, 192 (1963).
[33]S. Geltman, in *Topics in Atomic Collision Theory* (Academic, New York, 1969), p. 166.
[34]J. N. Bardsley and R. K. Nesbet, Phys. Rev. A 8, 203 (1973).
[35]D. W. Norcross and M. J. Seaton, J. Phys. B 6, 614 (1973).
[36]V. L. Jacobs and P. G. Burke, J. Phys. B 5, L67 (1972).
[37]S. Geltman, Astrophys. J. 136, 935 (1962).
[38]M. J. Seaton (private communication).
[39]S. Geltman, Phys. Rev. 104, 346 (1956).
[40]B. H. Armstrong, Phys. Rev. 131, 1132 (1963).
[41]T. A. Patterson, H. Hotop, and W. C. Lineberger (private communication).
[42]A. Kasdan and W. C. Lineberger, following paper, Phys. Rev. A 10, 1658 (1974).